International Journal of Advanced Engineering Research and Science (IJAERS)
Peer-Reviewed Journal
ISSN: 2349-6495(P) | 2456-1908(O)
Vol-12, Issue-7; Jul, 2025
Journal Home Page Available: https://ijaers.com/
Article DOI: https://dx.doi.org/10.22161/ijaers.127.4

Water Wave Transformation Model for Short and Long Waves

Syawaluddin Hutahaean

Ocean Engineering Program, Faculty of Civil and Environmental Engineering-Bandung Institute of Technology (ITB), Bandung 40132, Indonesia.
syawalf1@yahoo.co.id

Received: 20 Jun 2025,

Received in revised form: 15 Jul 2025,

Accepted: 19 Jul 2025,

Available online: 25 Jul 2025

***Keywords*— refraction-diffraction, shoaling, breaking, run-up**

***Abstract*—** *This research presents the formulation of a governing equation for water wave propagation, developed based on the three-dimensional Laplace equation and its velocity potential solution derived through the method of separation of variables. The resulting governing equation takes the form of a parabolic differential equation. The formulation is conducted without imposing limitations on wave amplitude or seabed slope, enabling the model to accommodate maximum wave amplitudes for a given wave period and a wide range of bathymetric gradients. As such, the model is applicable to both short waves and long waves, including tsunamis and sneaker waves. The proposed model effectively simulates key wave transformation processes such as refraction-diffraction, shoaling, breaking, and run-up. Additionally, it is capable of modeling wave overtopping over breakwaters induced by short waves.*

I. INTRODUCTION

Accurate wave condition data in coastal waters is essential for coastal structure design and sediment transport analysis. While deep-water wave conditions, unaffected by seabed features, can be obtained through measurements or hindcasting, such methods are impractical in shallow coastal zones due to spatial variability caused by bathymetric influences.

To address this, wave propagation in coastal regions is typically analyzed on a two-dimensional plane, accounting for hydrodynamic processes such as refraction, diffraction, shoaling, and breaking. Among the various models developed, the mild-slope equation has emerged as the most widely used. Originally proposed by Eckart (1952) and independently developed by Berkhoff (1972), this model was designed for gently sloping bathymetry. Subsequent advancements have extended its applicability to steeper slopes and incorporated factors such as wave-current interactions and nonlinearity. Notable contributors include Dingemans (1997), Porter (2003, 2006, 2020), Toubul et al. (2016), and others.

This research develops a wave refraction-diffraction model based on the three-dimensional Laplace equation. The resulting parabolic differential equation is amenable to numerical solutions via the Finite Difference Method and is applicable to steep bathymetry with maximum wave amplitude at a given wave period.

II. WEIGHTED TAYLOR SERIES AND WEIGHTING COEFFICIENT

This section introduces the weighted Taylor series as formulated by Hutahaean (2025a), which modifies the standard truncated Taylor series by incorporating first-order weighting coefficients for each derivative term.

Weighted Taylor series for function $f = f(x,t)$, where x is the horizontal axis and t is time

$$f(x+\delta x, t+\delta t) = f(x,t) + \gamma_{t,2}\delta t \frac{\partial f}{\partial t} + \gamma_{x,2}\delta x \frac{\partial f}{\partial x} \quad \ldots (1)$$

$\gamma_{t,2}$ and $\gamma_{x,2}$ are the first-order weighting coefficients, with base values $\gamma_{t,2} = 2.0$ and $\gamma_{x,2} = 1.0$. In this research, the values used are $\gamma_{t,2} = 1.998933$ and $\gamma_{x,2} = 0.998933$.
Weighted Taylor series for function $f = f(x,z,t)$, where x is the horizontal axis, z is the vertical axis and t is time,

$$f(x+\delta x, z+\delta z, t+\delta t) = f(x,z,t) + \gamma_{t,3}\delta t\frac{\partial f}{\partial t} + \gamma_{x,3}\delta x\frac{\partial f}{\partial x} + \gamma_{z,3}\delta z\frac{\partial f}{\partial z} \quad \ldots.(2)$$

$\gamma_{t,3}$, $\gamma_{x,3}$and $\gamma_{z,3}$ are weighting coefficients with base values of $\gamma_{t,3} = 3.0$, $\gamma_{x,3} = 2.0$ and $\gamma_{z,3} = 2.0$. The following values are used in this research: $\gamma_{t,3} = 3.098667$ and $\gamma_{x,3} = \gamma_{z,3} = 2.098667$.

The method for the calculation of the weighting coefficients are adopted from Hutahaean (2025a).

III. FORMULATION OF THE GOVERNING EQUATION

The governing equation is derived from the three-dimensional Laplace equation by substituting its analytical solution back into the equation. This involves accounting for the horizontal differentials of wave parameters and applying conservation and interrelation equations between the parameters involved.

3.1. 3D Laplace Equation

The general form of the three-dimensional Laplace equation is as follows.

$$\frac{\partial^2\phi}{\partial x^2} + \frac{\partial^2\phi}{\partial y^2} + \frac{\partial^2\phi}{\partial z^2} = 0 \quad \ldots(3)$$

$\phi(x,y,z)$ is velocity potential, x and y are horizontal axis, while z is the vertical axis, Fig (1).

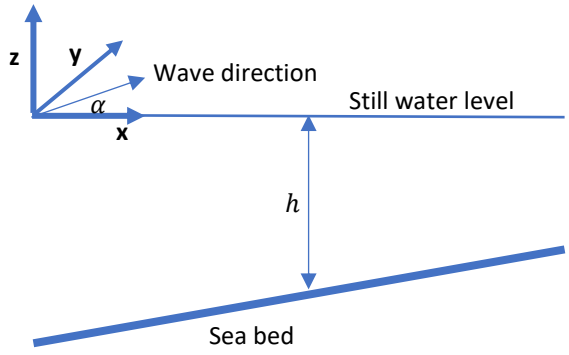

Fig (1). Coordinate System and Wave Angle Orientation.

3.2. Solution to the Laplace Equation

Using the method of separation of variables, the solution to the Laplace equation can be expressed as (Dean, 1991):

$$\phi(x,z,t) = G\,(\cos k(x\cos\alpha + y\sin\alpha) + \sin k(x\cos\alpha + y\sin\alpha))\cosh k(h+z)\sin\sigma t \quad \ldots(4)$$

At specific points where $\sin k(x\cos\alpha + y\sin\alpha) = \cos k(x\cos\alpha + y\sin\alpha)$, the velocity potential simplifies to:

$$\phi(x,z,t) = 2G\ \cos k(x\cos\alpha + y\sin\alpha)\cosh k(h+z)\sin\sigma t \quad \ldots(5)$$

For the velocity potential equations (4) and (5),

$\phi(x,z,t)$= velocity potential,

G = wave constant

k = wave number, where $k = \frac{2\pi}{L}$, L is wave-length

σ = wave angular frequency, where $\sigma = \frac{2\pi}{T}$, T is wave period.

α = wave propagation angle, Fig (1).

3.3. Wave Number Conservation Equation.

According to Hutahaean (2023), the wave number conservation equation is given by:

$$k\left(h + \frac{A}{2}\right) = \theta\pi \quad \ldots.(6)$$

A is wave amplitude, h is water depth and θ is deep water coefficient where $\tanh\theta\pi \approx 1$. The value of deep water coeffient determines breaker depth where smaller θ represents shallower breaker depth, vice versa. Using $\theta = 1.95$, results in $\frac{H_b}{h_b} = 0.78$, where H_b is the breaking wave heght and h_b is the breaking water depth. Using a deep-water coefficient of $\theta = 2.5$, where $\frac{H_b}{h_b} = 0.73$, wave heights in shallow waters near the coastline remain moderate.

The wave number conservation equation (Equation 6) governs the shoaling process, where decreasing water depth h leads to an increase in k and shorter wavelength.

3.4. Wave Amplitude Function.

Hutahaean (2023, 2025a) also introduced a wave amplitude function that defines the relationship among several wave parameters:

$$A = \frac{2Gk}{\gamma_{t,2}\sigma}\cosh\theta\pi\left(\tanh\theta\pi - \frac{\gamma_{x,2}kA}{2}\right) \quad \ldots(7)$$

$\gamma_{x,2}$ is the weighting coefficient from the weighted Taylor series in Equation (1).

This function inherently models wave breaking, which occurs when:

$$\tanh\theta\pi - \frac{\gamma_{x,2}kA}{2} = 0$$

From this, the breaking criterion can be derived as

$$\frac{H_b}{L_b} = \frac{2\tanh\theta\pi}{\gamma_{x,2}\pi} \quad \dots(8)$$

L_b is the breaking wave length. The incorporation of this breaking characteristic into the wave amplitude function ensures that wave breaking is automatically simulated in shoaling models using Equation (7) to evaluate changes in wave amplitude.

3.5. Refraction-Diffraction Equation.

By substituting Equation (4) into the Laplace equation (3), while allowing for spatial variations in the wave constants G, k and evaluating at the characteristic point, where $\sin k(x\cos\alpha + y\sin\alpha) = \cos k(x\cos\alpha + y\sin\alpha)$, obtaining

$$\frac{\partial^2 G}{\partial x^2} + \frac{\partial^2 G}{\partial y^2} = 0 \quad \dots(9)$$

Substituting Equation (5) into the Laplace equation (3), applying it at the same characteristic point, and incorporating Equation (9), yields:

$$\frac{\partial Gk\cos\alpha}{\partial x} + \frac{\partial G}{\partial x}k\cos\alpha + \frac{\partial Gk\sin\alpha}{\partial y} + \frac{\partial G}{\partial y}k\sin\alpha = 0$$

Neglecting $\frac{\partial\alpha}{\partial x}$ and $\frac{\partial\alpha}{\partial y}$, the following equation is obtained

$$2\frac{\partial G}{\partial x}k\cos\alpha + \frac{\partial k}{\partial x}G\cos\alpha + 2\frac{\partial G}{\partial y}k\sin\alpha + \frac{\partial k}{\partial y}G\sin\alpha = 0 \quad \dots(10)$$

Equation (10) is the foundational equation for the refraction-diffraction model. For waves propagating along the x, diffraction components are embedded in the third and fourth terms on the left-hand side.

To express Equation (10) in terms of wave number gradients $\frac{\partial k}{\partial x}$ and $\frac{\partial k}{\partial y}$. The wave amplitude function (Equation 7) and the wave number conservation equation (Equation 6) are utilized.

Wave amplitude function is written as,

$$A = Gk\lambda \quad \dots(11)$$

Where,

$$\lambda = \frac{2}{\sigma\gamma_{t,2}}\cosh\theta\pi\left(\tanh\theta\pi - \frac{\gamma_{x,2}kA}{2}\right) \quad \dots(12)$$

Differentiating Equation (11) with respect to horizontal axis x,

$$k\frac{\partial G}{\partial x} = \frac{1}{\lambda}\frac{\partial A}{\partial x} - G\frac{\partial k}{\partial x} \quad \dots(13)$$

Differentiating Equation (6) with respect to horizontal-x,

$$\frac{\partial A}{\partial x} = -\frac{2}{k}\left(h + \frac{A}{2}\right)\frac{\partial k}{\partial x} - 2\frac{\partial h}{\partial x} \quad \dots(14)$$

Substituting (14) to (13),

$$k\frac{\partial G}{\partial x} = -\left(\frac{2}{k\lambda}\left(h + \frac{A}{2}\right) + G\right)\frac{\partial k}{\partial x} - \frac{2}{\lambda}\frac{\partial h}{\partial x} \quad \dots(15)$$

Using the same procedure, the following is obtained.

$$k\frac{\partial G}{\partial y} = -\left(\frac{2}{k\lambda}\left(h + \frac{A}{2}\right) + G\right)\frac{\partial k}{\partial y} - \frac{2}{\lambda}\frac{\partial h}{\partial y} \quad \dots(16)$$

Substituting (15) and (16) to (10),

$$\cos\alpha\left(h + \frac{3A}{4}\right)\frac{\partial k}{\partial x} + k\frac{\partial h}{\partial x}\cos\alpha + \sin\alpha\left(h + \frac{3A}{4}\right)\frac{\partial k}{\partial y} + k\frac{\partial h}{\partial y}\sin\alpha = 0 \quad \dots(17)$$

Equation (17) governs wave refraction and diffraction, with the third and fourth terms representing diffraction effects.

3.6. Numerical Solution.

Equation (17) represents a parabolic differential equation that can be solved using the Finite Difference Method with a forward difference scheme. Equation (17) is rewritten as,

$$a_1\frac{\partial k}{\partial x} = -a_2\frac{\partial h}{\partial x} - a_3\frac{\partial k}{\partial y} - a_4\frac{\partial h}{\partial y} \quad \dots(18)$$

Where

$$a_1 = \cos\alpha\left(h + \frac{3A}{4}\right)$$

$$a_2 = k\cos\alpha$$

$$a_3 = \sin\alpha\left(h + \frac{3A}{4}\right)$$

$$a_4 = k\sin\alpha$$

In this research, the term $\frac{3A}{4}$ is replaced with $1.95\,A$ which corresponds to an increase in effective depth of $0.6H = 1.2A$. This modification accounts for the wave profile characteristics, which are cnoidal in deep water and solitary in shallow water (Hutahaean, 2024). This adjustment ensures

that the model remains applicable even in very shallow water or on land where the water depth h is negative, provided that the condition $(h + 1.95A) > 0$.

Equation (17) can be further expressed as

$$\frac{\partial k}{\partial x} = -\frac{1}{a_1}\left(a_2\frac{\partial h}{\partial x} + a_3\frac{\partial k}{\partial y} + a_4\frac{\partial h}{\partial y}\right) \quad \dots (19)$$

For very small δx, the relationship is

$$k_{x+\delta x} = k_x + \delta x\frac{\partial k}{\partial x} \quad \dots (20)$$

Hutahaean (2023) further proposed,

$$G_{x+\delta x} = e^{\ln G_x - \frac{1}{2}(\ln k_{x+\delta x} - \ln k_x)}$$

For equation (11),

$$\frac{\partial A}{\partial x} = \lambda k\frac{\partial G}{\partial x} + \lambda G\frac{\partial k}{\partial x} \quad \dots (21)$$

Where

$$\frac{\partial G}{\partial x} = \frac{G_{x+\delta x} - G_x}{\delta x}$$

The following is obtained

$$A_{x+\delta x} = A_x + \delta x\frac{\partial A}{\partial x} \quad \dots (22)$$

Once $k_{x+\delta x}$ and $A_{x+\delta x}$ is determined, $\sigma_{x+\delta x}$ can be calculated using (24),

$$\left(\sqrt{2} + \frac{k_{x+\delta x}A_{x+\delta x}}{\sqrt{2}}\tanh\theta\pi\right)\gamma_{t,3}\gamma_{t,2}\sigma_{x+\delta x}^2 = gk_{x+\delta x}\tanh\ \theta\pi$$

This shows that as waves propagate toward shallower regions, not only the wave amplitude and wave number change, but also the wave period.

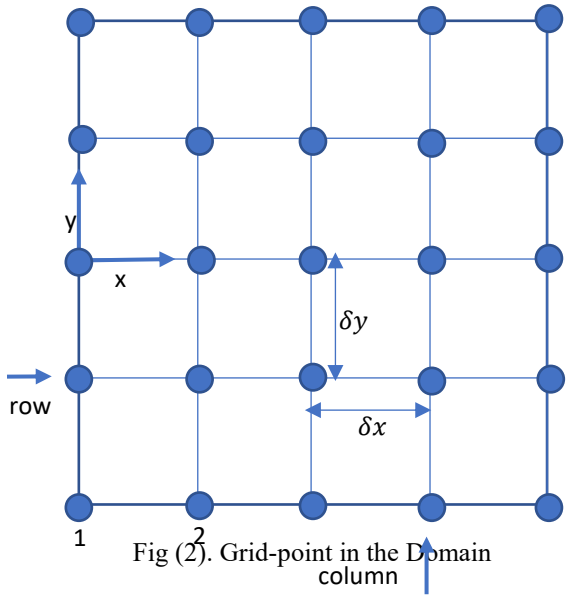

Fig (2). Grid-point in the Domain

The first column lies in deep water, where the deep-water wave amplitude A_0. Using A_0, k_0 and σ_0 can be calculated.

a. Calculation of deep-water wave number.

$$k_0 = \frac{\tanh\theta\pi}{\gamma_{x,2}A_0}\left(2 - \sqrt{2}\right) \quad \dots (23)$$

The derivation of this equation refers to Hutahaean (2025a)

b. Calculation of deep-water wave frequency

$$\left(\sqrt{2} + \frac{k_0A_0}{\sqrt{2}}\tanh\theta\pi\right)\gamma_{t,3}\gamma_{t,2}\sigma_0^2 = gk_0\tanh\ \theta\pi \quad \dots (24)$$

The derivation of this equation can be found in Hutahaean (2025b).

c. Calculation of G_0

Equation (10) can be reformulated for G

$$\lambda_0 = \frac{2}{\sigma_0\gamma_{t,2}}\cosh\ \theta\pi\left(\tanh\theta\pi - \frac{\gamma_x k_0A_0}{2}\right)$$

$$G_0 = \frac{A_0}{k_0\lambda_0} \quad \dots (25)$$

The calculations are conducted sequentially from column to column, whereby wave conditions at column x are used to compute wave parameters at column $x + \delta x$.

From the first column, values of k, A, G, σ and α at all points in the second column are determined. The spatial derivatives $\frac{\partial h}{\partial x}$, $\frac{\partial k}{\partial y}$ and $\frac{\partial h}{\partial y}$ is calculated in column 1. Similarly, a_1, a_2, a_3 and a_4 are calculated using data from the first column x. After k, A, G, σ are obtained in all points in the second column, wave angel α in all the points in column 2 are determined using the following equation.

$$\alpha_{x+\delta x} = -\operatorname{atan}\left(\cos\alpha_x\left(\frac{\partial C}{\partial y}\right)_x\right) \quad \dots (26)$$

where $C = \frac{L}{T} = \frac{\sigma}{k}$ is wave celerity. This equation is derived from the principle that wave direction is perpendicular to the tangent of the wave front.

Having determined all wave parameters at all points in the second column, the wave parameters at the third column are then calculated using the wave conditions at the second column. This process continues iteratively until wave conditions at the n column are obtained.

IV. MODEL OUTPUT EXAMPLE

In the following wave transformation analyses, the input parameters include a deep-water wave amplitude of $A_0 =$

1.2 m and incoming wave angel $\alpha_0 = 0^0$. Based on A_0 , the corresponding deep-water wave parameter k_0, σ_0 and G_0 are calculated, resulting in $L_0 = 12.86\ m$, $T_0 = 9.66$ sec., $h_0 = 15.47\ m$, $G_0 = 0.0018$ m.m/sec.

The computation utilizes the following weighting coefficients: $\gamma_{t,2} = 1.998933$, $\gamma_{x,2} = 0.998933$ and $\gamma_{t,3} = 3.098667$ and deep-water coefficient $\theta = 2.5$.

Grid-size δx and δy where $\delta x = \delta y$ are determined using the formulation provided by Hutahaean (2025c):

$$\frac{\delta x}{2}\frac{2\pi}{L} - \frac{\delta x^2}{3!}\left(\frac{2\pi}{L}\right)^2 - \frac{\delta x^3}{4!}\left(\frac{2\pi}{L}\right)^3 - \varepsilon_x = 0 \qquad \ldots (27)$$

Where $\varepsilon_x = 0.01$. This third-degree polynomial equation is solved using the Newton-Raphson iterative method, with the initial iteration value defined as:

$$\delta x = \frac{\varepsilon_x}{\pi} L \qquad \ldots (28)$$

4.1. Model Execution on Breakwater.

This section presents the model simulation applied to a steep-sloped bathymetry, specifically a breakwater structure, where the crest of the breakwater lies above the still water level. As shown in Figure (3), the bathymetric slope is calculated as $\frac{16-2}{20} = 0.7$, and the crest of the breakwater is situated 0.5 m above the still water level.

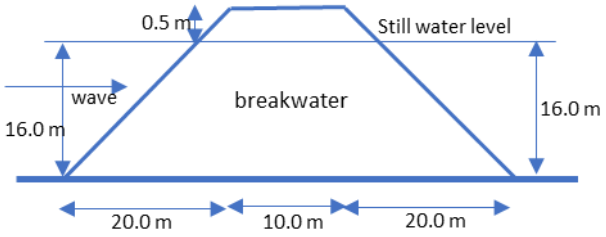

Fig (3) Breakwater cross section (non-scale)

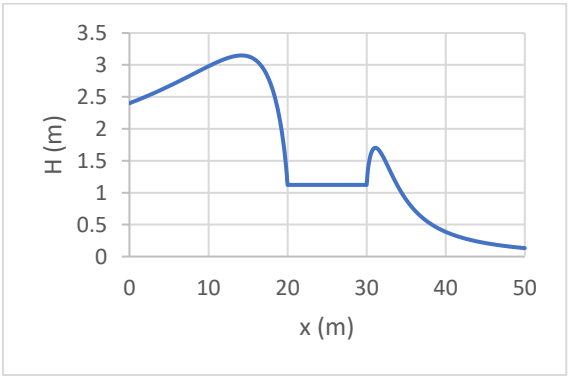

Fig (4) Wave height profile along the breakwater.

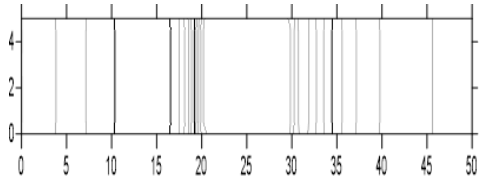

Fig (5) 2D contour wave height at the breakwater

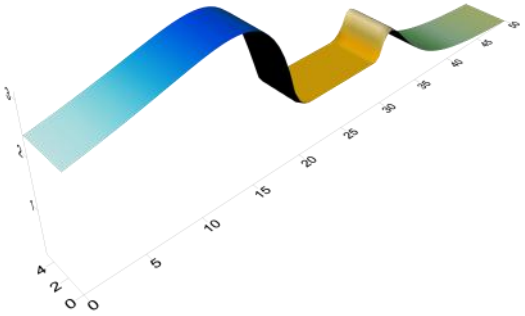

Fig (6) 3D contour wave height at the breakwater

As illustrated in Figures 4–6, shoaling occurs followed by wave breaking at a breaker depth of $h_{br} = 4.29\ m$, with breaker height $H_b = 3.15\ m$, where $\frac{H_{br}}{h_{br}} = 0.73$. At the crest of the breakwater, the wave height reduces to $H = 1.10\ m$. At the far end of the breakwater crest, the wave height increases to 1.70 m, and then gradually decreases to nearly zero as the water depth reaches 16.0 m. The wave height does not recover to its original value of 2.40 m, indicating the occurrence of a jet flow over the breakwater crest and a hydraulic jump at its far edge.

Additionally, this phenomenon reflects significant energy dissipation due to shoaling, breaking.

In the proposed model, wave energy dissipation is represented through the wave amplitude function given in Equation (7),

$$A = \frac{2Gk}{\gamma_{t,2}\sigma}\cosh\theta\pi\left(\tanh\theta\pi - \frac{\gamma_{x,2}kA}{2}\right) \qquad \ldots . (7)$$

The term $\left(\tanh\theta\pi - \frac{\gamma_{x,2}kA}{2}\right)$ where shallower water depth is followed by greater $\frac{\gamma_{x,2}kA}{2}$, resulting smaller $\left(\tanh\theta\pi - \frac{\gamma_{x,2}kA}{2}\right)$. Smaller wave amplitude A results in energy loss when $\frac{\gamma_{x,2}kA}{2}$ increases during the shoaling. This phenomenon indicates energy loss associated with wave shoaling. At the crest of the breakwater, where the effective water depth is extremely shallow, the wave number k becomes large. As a

result, substantial energy loss occurs even though the wave amplitude remains relatively small. When the waves propagate from the breakwater crest toward deeper water, they are unable to regain their original height due to the insufficient residual energy and water mass.

These simulation results demonstrate that the model effectively captures key wave transformation processes such as shoaling, breaking, and run-up, and is capable of being applied to highly variable and steep bathymetric slopes.

4.2. Model Implementation on a Headland (Tanjong)

In this section, the model is applied to a domain with complex bathymetry where waves are subject to both refraction and diffraction. The bathymetric configuration of the Tanjong (headland) area, illustrated in Figure (7), is used for the simulation. The results, presented in Figures (8) and (9), show clear evidence of wave refraction toward the center of the headland. These findings confirm that the model is capable of accurately simulating wave refraction and diffraction processes, in addition to shoaling and breaking, even under complex coastal configurations.

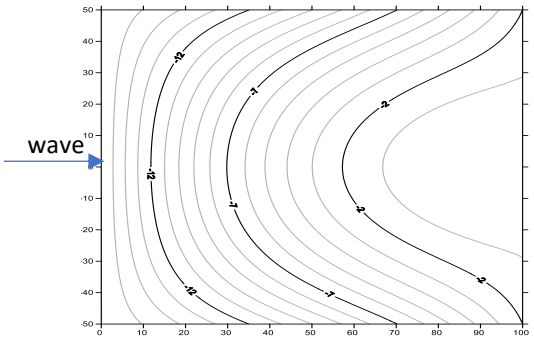

Fig (7) Bathymetric contours of the Tanjong area.

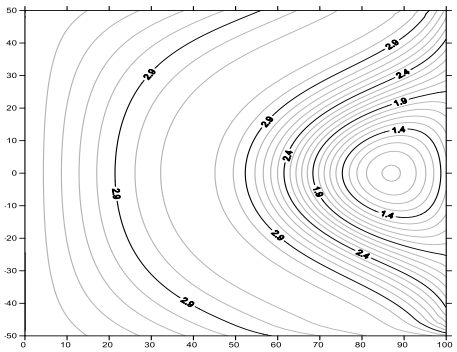

Fig (8) 2D contour wave height at the Tanjong area.

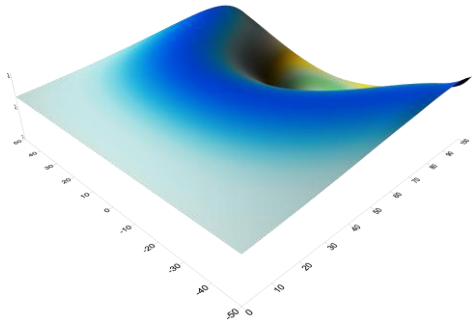

Fig (9) 3D contour wave height at the Tanjong area.

4.3. Long-Wave Propagation Analysis.

This section presents the application of the model to the simulation of long-wave propagation. The primary distinction between short-wave and long-wave simulations lies in the equations used to compute the deep-water wavelength and the corresponding deep-water coefficient. For the long-wave scenario, a deep-water coefficient of $\theta = 0.124$, is adopted, and the deep-water wave number is calculated using the formulation proposed by Hutahaean (2025b), as shown in Equation (28):

$$k_0 = \frac{\theta\pi}{\left(h_0 + \frac{A_0}{2}\right)} \quad \ldots (29)$$

In this context, the term “deep water” refers to the depth at the offshore boundary where the calculation begins or the location where wave generation occurs. Long-wave events represented in this research include tsunamis and sneaker waves, the latter also referred to as mini-tsunamis.

The wave period in deep water is computed using Equation (24), while the primary wave input for this simulation is the deep-water wave amplitude. Additional inputs include bathymetric data and the deep-water depth h_0.

In the present simulation, a deep-water wave amplitude of $A_0 = 0.5\ m$, The corresponding bathymetric cross-section is illustrated in Figure (10).

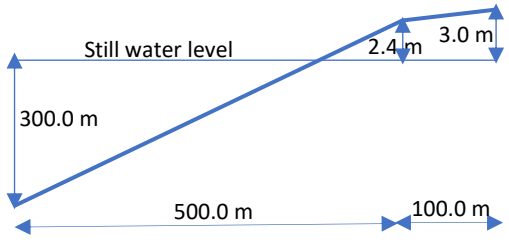

Fig (10) Bathymetry cross-section for long-wave simulation (non-scale).

The bathymetric profile shown in Figure (10) begins at a deep-water depth of $h_0 = 300\ m,$ to $h = -2.4\ m$, or 2.40 m above the still water level at zero elevation, ending at $h = -3.0\ m$, or topographic elevation of +3.00 m above the still water level. In this context, water depth negative is the land above the still water level. With $A_0 = 0.5\ m$, the followings are obtained: $L_0 = 2431.452\ m$ or $k_0 = 0.0026/m$ and $T_0 = 191.783\ sec.$ or $\sigma_0 = 0.0328/sec.$ The results of the wave transformation analysis are presented in Fig (11) 2D contour wave height, Fig (12) 3D contour wave height and Fig (13) wave height to water depth.

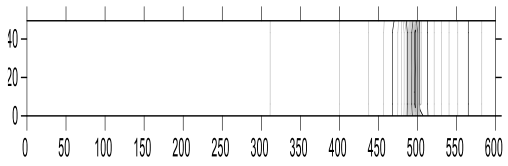

Fig (11) 2D contour wave height.

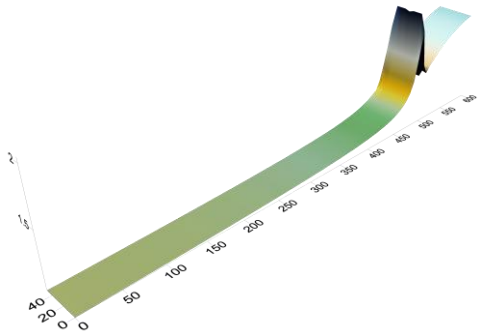

Fig (12) 3D contour wave height

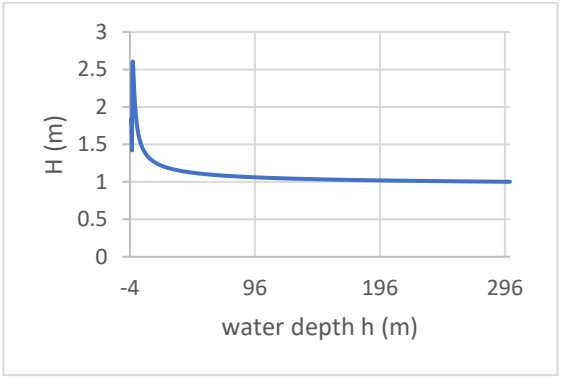

Fig (13) Wave height as a function of water depth.

In Figure (13), negative water depths indicate land regions above the SWL. Wave breaking is observed on land at a topographic elevation of $e = +1.80$ m, with a breaking wave height $H_{br} = 2.61$ m. Run-up extends to a maximum elevation of $e = +3.0\ m$, during which the wave height progressively decreases to 1.40 m. If the land surface is flat at this elevation, inundation occurs, characterized by a jet flow with a flow-depth of 1.4 m.

These results demonstrate that the model effectively captures the physical processes of shoaling, breaking, and run-up under long-wave conditions, including extreme events such as tsunamis and sneaker waves.

V. CONCLUSION

As demonstrated, the model is capable of simulating key phenomena associated with wave propagation in shallow waters, including shoaling, breaking, refraction-diffraction, and run-up. Overall, the governing equations employed in the model effectively capture the transformation processes of water waves.

In conclusion, the considerable destructive power of tsunamis in coastal zones and inland areas can primarily be attributed to the generation of jet flows characterized by extremely high velocities. Similarly, the damage observed on breakwaters as a result of overtopping is also caused by such high-velocity jet flows.

REFERENCES

[1] Eckart, C. (1952). The propagation of gravity waves from deep to shallow water. Circular 20, National Bureau of Standards: 165-173, Bibcode: 1952grwa.conf..165E

[2] Berkhoff, J.C.W. (1972). Computation of combined refraction-diffraction. Proceeding 13th International Conference on Coastal Engineering, Vancouver, pp. 472-490, doi.10.9753/ice. v13.23.

[3] Dingemans, M.W. (1997). Water wave propagation over uneven bottoms. Advanced series on Ocean Engineering, vol.13 World Scientific, Singapore. ISBN 981—02-0427-2, OCLC 36126836, 2 Parts 967 pages.

[4] Porter, D. (2003). The mild-slope equations. Journal of Fluid Mechanics. 494: 51-63, Bibcode:2003JFM…494….51P, doi

[5] Porter, R. & Porter, D. (2006). Approximation to the scattering of water waves by steep topography. J.Fluid Mech. 562, 279-302. CrossRef Google Scholar.

[6] Toubul, J., Charland, J.,Rey, V., Bellibassakis (2016). Extended mild-slope equation for surface waves interacting with a vertically sheared current. Coas.Eng.116-, 78-88. CrossRef Google Scholar.

[7] Porter, D. (2020). The mild-slope equations: a unified theory. Published online by Cambridge University Press: 29 January 2020.

[8] Hutahaean, S. (2025a). New Weighted Taylor Series for Water Wave Energy Loss and Littoral Current Analysis. International Journal of Advance Engineering Research and Science (IJAERS). Vol. 12, Issue 1; Jan, 2025, pp 27-39. Article DOI: https://dx.doi..org/10.22161/ijaers.121.3.

[9] Dean, R.G., Dalrymple, R.A. (1991). Water wave mechanics for engineers and scientists. Advance Series on Ocean Engineering.2. Singapore: World Scientific. ISBN 978-981-02-0420-4. OCLC 22907242.

[10] Hutahaean, S. (2023). Water Wave Velocity Potential on Sloping Bottom in Water Wave Transformation Modeling. International Journal of Advance Engineering Research and Science (IJAERS). Vol. 10, Issue 10; Oct, 2023, pp 149-157. Article DOI: https://dx.doi..org/10.22161/ijaers.1010.15

[11] Hutahaean, S. (2024). Periodic Water Wave: Cnoidal and Solitary Profiles. International Journal of Advance Engineering Research and Science (IJAERS). Vol. 11, Issue 11; Nov, 2024, pp 28-34. Article DOI: https://dx.doi..org/10.22161/ijaers.1111.4.

[12] Hutahaean, S. (2025b). Long Wave Analysis Using Velocity Potential Equation. International Journal of Advance Engineering Research and Science (IJAERS). Vol. 12, Issue 6; Jun, 2025, pp 59-68. Article DOI: https://dx.doi..org/10.22161/ijaers.126.6.

[13] Hutahaean, S. (2025c). Diffraction Model on the Breakwater Gap Based on Velocity Potential Equation. International Journal of Advance Engineering Research and Science (IJAERS). Vol. 12, Issue 5; May, 2025, pp 39-44. Article DOI: https://dx.doi..org/10.22161/ijaers.125.6.